Impacts of wall conditions on flame acceleration at the early stages of burning in channels

Mohammed AlKhabbaz,[1] Furkan Kodakoglu,[1] Damir Valiev,[2] and V'yacheslav Akkerman[1,*]

[1]*Center for Innovation in Gas Research and Utilization (CIGRU), Center for Alternative Fuels, Engines and Emissions (CAFEE), Computational Fluid Dynamics and Applied Multi-Physics Center, Department of Mechanical and Aerospace Engineering, West Virginia University, Morgantown, West Virginia 26506, USA*

[2]*Center for Combustion Energy, Department of Energy and Power Engineering, Tsinghua University, Beijing 100084, China*

(Received 15 August 2018; accepted 3 January 2022; published 31 January 2022)

The role of mechanistic (shear stress) and thermal wall conditions on the scenario of finger-shaped flame acceleration at the early stages of burning in channels is studied by means of computational simulations of the reacting flow equations involving fully compressible hydrodynamics, transport properties (heat conduction, diffusion, and viscosity), and chemical kinetics imitated by a one-step Arrhenius reaction. Specifically, free-slip walls (i.e., no shear stress at the walls) or nonslip walls (with shear stress) are considered as the mechanistic conditions, while the options for the thermal boundaries include adiabatic walls or isothermal walls of various temperatures. The parametric study involves variations of the channel widths, the thermal expansion ratios, and isothermal wall temperatures for the cases of both slip and nonslip wall conditions. It is shown that the difference between the effects of slip and nonslip walls is generally small during the early stages of burning, before a flame skirt contacts a sidewall. Thereafter, wall friction may play the role; in particular, it may distort or even prevent the formation of a tulip flame front. As for the thermal boundaries, while the finger flame dynamics in adiabatic channels is oftentimes similar to that in isothermal ones, the wall temperature has an impact on flame acceleration such that a flame tends to accelerate faster in hotter channels. Moreover, for isothermal walls preheated to a high temperature, emergence and propagation of an octopuslike flame front are observed. This feature is devoted to the formation of the secondary flame segments near very hot sidewalls, due to a high wall temperature. The impact of thermal expansion on the flame acceleration rate is significant for any wall conditions; it is slightly stronger for isothermal walls, and the flame front approaches the sidewalls faster at a lower thermal expansion ratio. Variation of the channel width shows a small impact in the case of adiabatic walls as well as preheated isothermal walls, but it provides a significant influence on flame propagation in a channel with isothermal walls kept at an initial fuel temperature. At the same time, the role of the channel width is practically the same for both slip and nonslip walls. Overall, the present work verifies and underlines the limitations of the previous theoretical models and computational studies of finger flame acceleration that employed adiabatic slip walls.

DOI: 10.1103/PhysRevFluids.7.013201

*Vyacheslav.Akkerman@mail.wvu.edu

I. INTRODUCTION

Understanding of premixed flame acceleration commands both fundamental interest and practical relevance. First, being often hazardous and destructive, rapid flame acceleration can be potentially utilized to achieve better efficiency of a combustor, in particular, in pulse- or rotation-detonation engines [1]. Second, careful inferences are required to reduce the risks of accidental events in facilities operating with flammable gas or/and combustible dust [2]. Among various configurations of a combustor, tubes or channels are most oftentimes used in the studies of flame acceleration and the deflagration-to-detonation transition (DDT) [3]. Presumably, this is (i) because a channel geometry is the simplest to study, from a theoretical viewpoint, and (ii) because it is in this geometry that the acceleration rate may be the highest and/or high enough to trigger detonation.

Among various mechanisms of flame acceleration in channels [4–21], in the present work, we deal with finger flame acceleration, which has been under the spotlight in a number of works [4,7–20]. For the first time, this phenomenon was studied experimentally by Ellis [7], for a flame in a closed cylindrical tube. However, what is better recognized are the experiments of Clanet and Searby [4], with four different stages of flame propagation observed, namely: (i) hemispherical flame expansion, (ii) exponential acceleration of a finger-shaped flame that lasts until the flame "skirt" contacts the sidewalls, (iii) flame deceleration due to the decrease in the flame surface area, and (iv) presence of acoustic effects after the so-called "tulip flame" formation. Initial acceleration, associated with the transition between stages (i) and (ii), occurs when an initially hemispherical flame front starts approaching the sidewalls such that the axial flow velocity exceeds the radial one considerably. For other experiments on the subject, the reader can be referred to the studies by Xiao *et al.* [14–16] or Kuznetsov *et al.* [17,18] and references therein.

The dynamics and morphology of a finger flame front along with other parameters such as the acceleration time interval, the evolution of the position and velocity of the flame tip, as well as its acceleration rate have been identified, analytically and computationally, by Bychkov *et al.* [13]. Subsequently, the effect of gas compressibility on finger flame acceleration was investigated by Valiev *et al.* [18], with the conclusion that gas compression moderates the flame acceleration rate noticeably. Reference [13] also found that finger flame acceleration is scale invariant, i.e., Reynolds independent, which makes it equally strong for microchannels and mining passages. Demir *et al.* [19,20] adopted the finger flame acceleration mechanism to coal mines, combining it with the Darrieus-Landau combustion instability, and they arrived at the conclusion that several orders of magnitude increase in the flame propagation velocity, due to the instability plus the finger flame acceleration scenario, may trigger detonation, which is a disaster in accidental burning events in the coal-mining industry. It is noted, in this respect, that turbulence and combustion instabilities may influence propagation of a finger-shaped flame in a large-scale conduit such as a mining passage [22], though their impacts on the rate of flame acceleration are still unclear. Moreover, it is noted that most of the theoretical and computational studies of flame acceleration in channels [6,13,18–21] involved a number of simplifying assumptions such as adiabatic and free-slip or nonslip wall boundary conditions. However, the walls are neither adiabatic nor slip in practice, and wall conditions may significantly impact flame propagation. Han *et al.* [22] considered an adiabatic and nonslip open channel, with a planar flame ignition at the closed end of the channel. The authors of Ref. [22] considered various channel widths, namely, micro- and macrochannels, and compared the two different modes of flame propagation. Ivanov *et al.* [23] performed computational simulations of hydrogen-oxygen flame acceleration in two-dimensional (2D) channels of various widths using a detailed chemical model. The authors of Ref. [23] noted that the features of flame acceleration depend on the width of the channel. Dzieminska and Hayashi [24] studied an interplay between a shock wave and a boundary layer for the autoignition in the boundary layer for the channels with adiabatic and nonslip walls. In their simulations, the authors of Ref. [24] employed a detailed chemical reaction model (with 8 species and 18 reactions) and concluded that cooling down of the walls may prevent overheating of the boundary layer and possible DDT. Employing a detailed chemical kinetics, Machida *et al.* [25] performed three-dimensional (3D) computational simulations

of flame propagation in a rectangular channel, with isothermal and nonslip walls, filled with a hydrogen-oxygen mixture. The authors of Ref. [25] highlighted that flames propagate qualitatively similar in 2D and 3D geometries, until the transition to detonation; however, the time and location of the local explosions were different. Another comparison of 3D and 2D simulations of flame propagation in a channel was conducted by Ivanov *et al.* [26], with the conclusion that 2D cross sections of 3D simulations exhibit similar hydrodynamic flow pictures to those obtained in 2D simulations. The effect of the heat losses through the walls and the difference between free-slip and nonslip wall conditions have been studied for the acceleration mechanism driven by wall friction [27,28]. Ott *et al.* [29] studied premixed acetylene-air flame propagation in 2D channels, with a planar flame ignition at the closed side of the open channel. The authors of Ref. [29] employed adiabatic or isothermal walls and arrived at the conclusion that the growth of the boundary layer promoted the flame propagation speed for both thermal conditions. However, acceleration was slower in isothermal channels and, in some cases, heat losses even led to flame deceleration. Gamezo and Oran [28] studied the impact of the wall temperature on the propulsion characteristics and pointed out the importance of the proper selection of an insulation material for the efficiency of a propulsion device. The computational platform used in Ref. [28] was capable of introducing three types of boundary conditions, namely: adiabatic walls, isothermal walls, and walls set with a heat loss coefficient, which can vary to represent various insulation materials. The study [28] clearly demonstrated that the adiabatic and isothermal conditions are two opposite limits, while the practical reality lies in between these limits. It was found that with the increase in such a heat loss coefficient, the heat loss from the burnt matter to the walls mitigates flame acceleration. For isothermal cases, no significant acceleration was reported. Overall, isothermal walls provide a considerable impact on flame acceleration induced by wall friction: the exponential acceleration trend inherent to adiabatic conditions [21] is replaced by almost linear acceleration for isothermal wall conditions. Moreover, extinction may occur when a channel is very narrow. Hackert *et al.* [30] also investigated the effects of thermal boundary conditions on the flame shape and velocity, with a particular focus on the flame quenching distance in ducts. It was noted that the closer the duct to the adiabatic conditions is, the faster the flame is; however, the effect of internal radiation may further increase the burning rate even in the case of adiabatic boundary conditions. Specifically, internal radiation diminishes a quenching distance and promotes flame acceleration, while external radiation promotes heat transfer and increases a quenching distance. Among other studies to be mentioned, Brailovsky and Sivashinsky [31] developed a theoretical model to describe flame acceleration by introducing a friction parameter for burning in tubes. According to Ref. [31], hydraulic resistance exerts a destabilizing impact on flame propagation that can cause a transition from uniform propagation to gradual acceleration. While the model [31] neglected heat losses, Kagan *et al.* [27] extended the study [31] to account for this effect and concluded that heat losses tend to reverse the effects of hydraulic resistance and that the impact of heat losses is as strong as that of hydraulic resistance. Norton and Vlachos [32] reported that the channel walls with high thermal conductivity lead to a larger hot area for external heat transfer, making the global-like extinction more susceptible. Daou and Matalon [33] stated that excessive heat losses could cause total flame extinction in narrow channels, but only partial flame extinction in wider ones. In the latter case, a flame persists in the center of a channel. Gauthier and Bergthorson [34] considered various convective heat-transfer coefficients at the inner and outer wall surfaces of the tubes of various diameters, and they concluded that an increase in the external heat loss reduces the flame propagation velocity.

In summary, it is observed that the impact of wall conditions on flame propagation can be significant, especially when a flame propagates near a wall [28,35–38]. Will it be the case for finger flame acceleration at the initial stages of burning in channels? The previous works on finger flame acceleration [13,18–20] could not answer this question as they employed adiabatic, free-slip walls. Consequently, we address this point in the present work by means of extensive computational simulations of the reacting flow equations with fully compressible hydrodynamics and chemical kinetics imitated by a one-step Arrhenius reaction. Specifically, the effect of heat losses on finger flame acceleration is scrutinized by comparing the cases of isothermal slip walls at

different temperatures, to each other, and to that with adiabatic walls. In addition, the situations of slip and nonslip walls are also compared. The parametric study includes variations of the channel width and the thermal expansion ratio. Unlike the previous works, it is shown that termination of flame acceleration and formation of a tulip flame shape can be blocked by wall friction, which, however, provides extra acceleration. Also, heat losses tend to moderate flame acceleration in the presence of "cold" walls (kept at the initial fuel temperature); however, such an effect diminishes as the wall temperature increases.

II. DESCRIPTION OF THE NUMERICAL SIMULATIONS

We performed the computational simulations of the 2D compressible Navier-Stokes equations for unsteady reactive flows.

A. Governing equations

The governing equations are those for the balance of mass (the equation of continuity), momentum, energy, and species, and in the general form for a 2D Cartesian geometry they read

$$\frac{\partial}{\partial t}\rho + \frac{\partial}{\partial x_i}(\rho u_i) = 0, \tag{1}$$

$$\frac{\partial}{\partial t}(\rho u_i) + \frac{\partial}{\partial x_j}(\rho u_i u_j + \delta_{i,j}P - \zeta_{i,j}) = 0, \tag{2}$$

$$\frac{\partial}{\partial t}\left(\rho\varepsilon + \frac{1}{2}\rho u_i u_j\right) + \frac{\partial}{\partial x_i}\left(\rho u_i h + \frac{1}{2}\rho u_i u_j u_j + q_i - u_j\zeta_{i,j}\right) = 0, \tag{3}$$

$$\frac{\partial}{\partial t}(\rho Y) + \frac{\partial}{\partial x_i}\left(\rho u_i Y - \frac{\mu}{Sc}\frac{\partial Y}{\partial x_i}\right) = -\frac{\rho Y}{\tau_R}\exp(-E_a/R_u T), \tag{4}$$

where Y represents the mass fraction of the fuel mixture; $\varepsilon = QY + c_v T$ is the specific internal energy; $h = QY + c_p T$ is the specific enthalpy; $Q = c_p T_f(\Theta - 1)$ is the specific energy release from the reaction, where $\Theta = \rho_f/\rho_b = T_b/T_f$ designates thermal expansion in the burning process. We took $\Theta = 8$, typical for propane-air burning, as the "master case" of the numerical simulations, and then compared the results to the cases of smaller, $\Theta = 5$, and larger, $\Theta = 10$, expansion ratios. As for other parameters in Eqs. (1)–(4), $c_v = 5R_u/2M$ and $c_p = 7R_u/2M$ are the specific heats at constant volume and pressure, respectively, where $R_u = 8.31$ J/(mol K) is the universal gas constant, and the molar masses of the fuel-air mixture and the burnt matter are assumed to be equal, $M = 2.9 \times 10^{-2}$ kg/mol. The ideal gas model was implemented for both burned and unburned gases such that the equation of state reads $P = \rho R_u T/M$, with the initial pressure $P_f = 10^5$ Pa, temperature $T_f = 300$ K, and density $\rho_f = 1.16$ kg/m^3. The stress tensor $\zeta_{i,j}$ and the energy diffusion vector q_i are given by

$$\zeta_{i,j} = \mu\left(\frac{\partial u_i}{\partial x} + \frac{\partial u_j}{\partial x_i} - \frac{2}{3}\frac{\partial u_k}{\partial x_k}\delta_{i,j}\right), \quad q_i = -\mu\left(\frac{c_p}{\mathrm{Pr}}\frac{\partial T}{\partial x_i} + \frac{Q}{\mathrm{Sc}}\frac{\partial Y}{\partial x_i}\right), \tag{5}$$

where $\mu = 2.38 \times 10^{-5}$ Ns/m^2 is the dynamic viscosity, and Pr and Sc are the Prandtl and Schmidt numbers, respectively. To avoid the diffusional-thermal instability, in the present work we took $\mathrm{Pr} = \mathrm{Sc} = 0.7$ such that their ratio (the Lewis number) is unity, $\mathrm{Le} = \mathrm{Pr}/\mathrm{Sc} = 1$. In order to avoid the influence of gas compressibility, a relatively low initial Mach number, associated with flame propagation, was employed in such a way that $\mathrm{Ma} \equiv U_f/c_s = 10^{-3}$, where $c_s = 347$ m/s is the speed of sound. From this relation, the unstretched laminar flame velocity is calculated to be $U_f = 34.7$ cm/s. Once U_f is known, the flame thickness L_f can be conventionally defined as $L_f = \mu/\mathrm{Pr}\rho_f U_f \approx 5.9 \times 10^{-5}$ m. However, it is emphasized that the quantity L_f, defined in this way, is just a mathematical parameter of length dimension, while the real width of the burning zone,

determined by the temperature gradient, may exceed L_f by a factor of 4∼5 [39,40]. In this light, L_f characterizes the active reaction zone rather than the whole flame thickness [40].

According to Eq. (4), the chemical reaction is imitated by a one-step irreversible reaction obeying the Arrhenius law, with the activation energy E_a and the constant of time dimension τ_R. In the present work, we employed $E_a = 7R_uT_b$. The factor τ_R was adjusted to obtain a particular value of the planar flame speed U_f by solving the associated eigenvalue problem [21]. For instance, for $U_f = 34.7$ cm/s we set $\tau_R = 4.06 \times 10^{-8}$ s. The total burning rate has been calculated as [6]

$$U_w = \frac{1}{\rho_f H} \int \frac{\rho Y}{\tau_R} \exp(-E_A/R_uT)dxdz. \tag{6}$$

Another important characteristic of flame propagation is the flame-tip velocity in the laboratory reference frame, $U_{\text{tip}} \equiv dZ_{\text{tip}}/dt$.

A flame propagates in a long 2D channel of width $2H$. In this respect, the major dimensionless quantities of this study are the Reynolds number associated with flame propagation, $\text{Re} \equiv HS_L/\nu = H/L_f\text{Pr} = H/L_f$ (being actually the scaled channel half-width), the scaled time $\tau \equiv U_f t/H$, the instantaneous scaled flame-tip position Z_{tip}/H, its scaled velocity U_{tip}/U_f, and the instantaneous scaled burning rate U_w/U_f. In the postprocessing–analysis of the simulation data, in the present work, the location of the flame front has been localized by finding the locus (loci) of the maximum reaction rate.

It is noted that while detailed chemistry is certainly important for accurate simulations of the combustion processes, a one-step chemical model is conventionally applicable to the problems like that addressed in the present work—as long as we investigate the dimensionless quantities. Indeed, we are interested in the corrugated flame shape and its velocity as compared to the planar flame shape and velocity—instead of the dimensional value of the flame velocity. Consequently, "chemistry" is embedded here into the planar flame velocity U_f (which, in turn, is a function of E_a, Q, and τ_R). Moreover, in the present work, we investigate the impact of thermal and mechanistic wall conditions as compared to the previous studies on finger flame acceleration [13,18], both of which employed adiabatic, slip walls and one-step chemistry. Consequently, it was fully logical to employ here the same solver with the same one-step chemical model as in Refs. [13,18]—in order to *distinguish* the impacts of nonslip walls and isothermal walls. Otherwise, it would be hard to distinguish these impacts: new features might be devoted to the changes in a chemical model.

B. Boundary conditions

Different wall boundary conditions are employed in the numerical simulations to study their influence on flame acceleration. Specifically, we assume semiopen channels such that one end is open while the other is closed, and the embryonic flame is ignited at the channel centerline, at the closed end, and it propagates toward the open one. The employed boundary conditions read as follows:

(i) The free-slip walls are implemented by $\boldsymbol{n} \cdot \boldsymbol{u} = 0$, where $\boldsymbol{n}$ is the normal vector to the walls.

(ii) The nonslip walls are implemented by $\boldsymbol{u} = 0$.

(iii) The adiabatic walls are represented by $\boldsymbol{n} \cdot \nabla T = 0$.

(iv) The isothermal wall temperatures T_w are set in the range $298\ \text{K} \leqslant T_w \leqslant 1000\ \text{K}$.

C. Numerical scheme

The numerical scheme employed in the solver is based on the finite-volume method, being second-order accurate in time and fourth-order in space for the convective terms, and second-order in space for the diffusive terms. The boundary conditions have the same order of approximation as the overall numerical scheme, through the usage of the ghost cell technique. Consequently, the overall order of approximation is expected to be close to 2. The solver was first developed

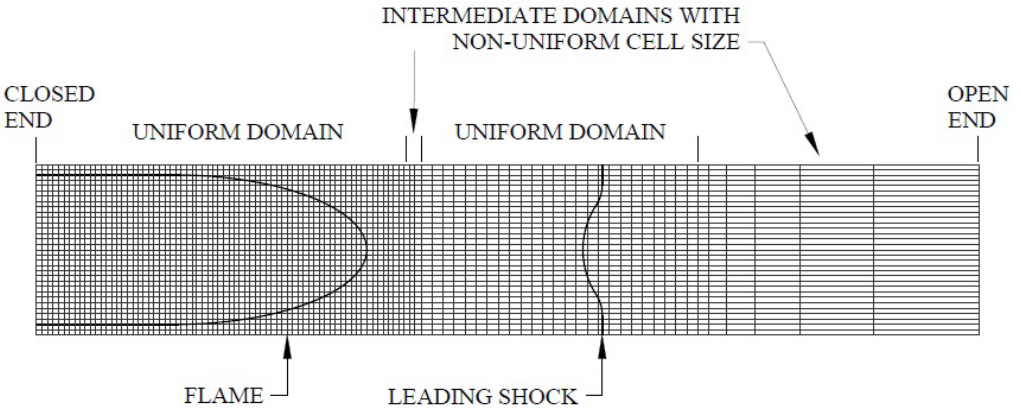

FIG. 1. The sketch of the grid used in the numerical simulations.

at Volvo Aero and was subsequently employed for academic use. More details of the numerical scheme can be found in Refs. [6,18]. The channel is assumed to be long enough such that its length does not influence flame propagation. A schematic of a typical dynamic mesh employed in the simulations is illustrated in Fig. 1. The numerical mesh consists of structured rectangular grids, with the grid walls parallel to each Cartesian axis. Additionally, the grid is uniform in the z-direction. In this study, we use an adaptive grid with a uniform grid size of $0.2\,L_f$ near the flame front. Outside the region of the fine grid, the mesh size increased gradually, with a 2% change in size between the neighboring cells. In order to keep the flame and pressure waves in the zone of the fine grid, we implemented a periodical mesh reconstruction during the simulation run. Sufficiency of such a grid had been successfully tested [18], but here we also validated our mesh for strongly curved flames in the acceleration process. Specifically, an extra resolution test has been performed for a flame with a thermal expansion ratio $\Theta = 8$ propagating in a channel of half-width $H = 20\,L_f$. The grid size has been varied in the range $0.1\,L_f \leqslant \Delta z_f \leqslant 0.8\,L_f$; see Fig. 2 and Table I. Specifically, in Table I we compare the scaled flame-tip positions $Z_{\rm tip}/H$ at the same scaled time instant $\tau = U_f t/H = 0.25$. Also, we checked the time instants corresponding to the maximal values of the scaled total burning rate U_w/U_f. Furthermore, the $\Delta U_{w,\max}/U_f$ increments are calculated from Table I as $\Delta U_{w,\max(i)} = U_{w,\max(i)} - \Delta U_{w,\max(i-1)}$, where the increments for the scaled time and the scaled flame-tip positions are calculated in the same manner. According to Ref. [41], the degree of convergence supposedly correlates with the order of the truncation rate decay, given by [41]

$$\check{p} = \ln\left|\frac{\check{U}_3 - \check{U}_2}{\check{U}_2 - \check{U}_1}\right| \Big/ \ln(\check{r}), \tag{7}$$

where $\check{U}_1$, $\check{U}_2$, and $\check{U}_3$ are the solutions provided by the coarse, medium, and fine grids, respectively, and $\check{r} = \Delta z_{f,2}/\Delta z_{f,1} = \Delta z_{f,3}/\Delta z_{f,2}$ is the (constant) refinement ratio. In particular, the quantities of $Z_{\rm tip}$ in Table I provide the following estimations for the order of the truncation rate decay: for $\Delta z_f = 0.8, 0.4, 0.2$, Eq. (7) yields $\check{p} = 1.42$, while for $\Delta z_f = 0.4, 0.2, 0.1$, it gives $\check{p} = 3.9$. It is noted that the average between the two quantities, $\check{p} = 2.66$, reasonably agrees with the overall order of approximation, slightly exceeding 2.

Figure 2 is a graphical representation of the resolution test. Here, $Z_{\rm tip}/H$ [Fig. 2(a)] and U_w/U_f [Fig. 2(b)] are plotted versus the scaled time τ, thereby demonstrating good convergence with the decrease of the grid size for the flame-tip position, especially at the early stages of burning. Overall, Table I and Fig. 2 certify that the chosen grid of size $0.2\,L_f$ is appropriate for this type of simulations. It is recalled, in this respect, that L_f characterizes the active reaction zone rather than the whole flame

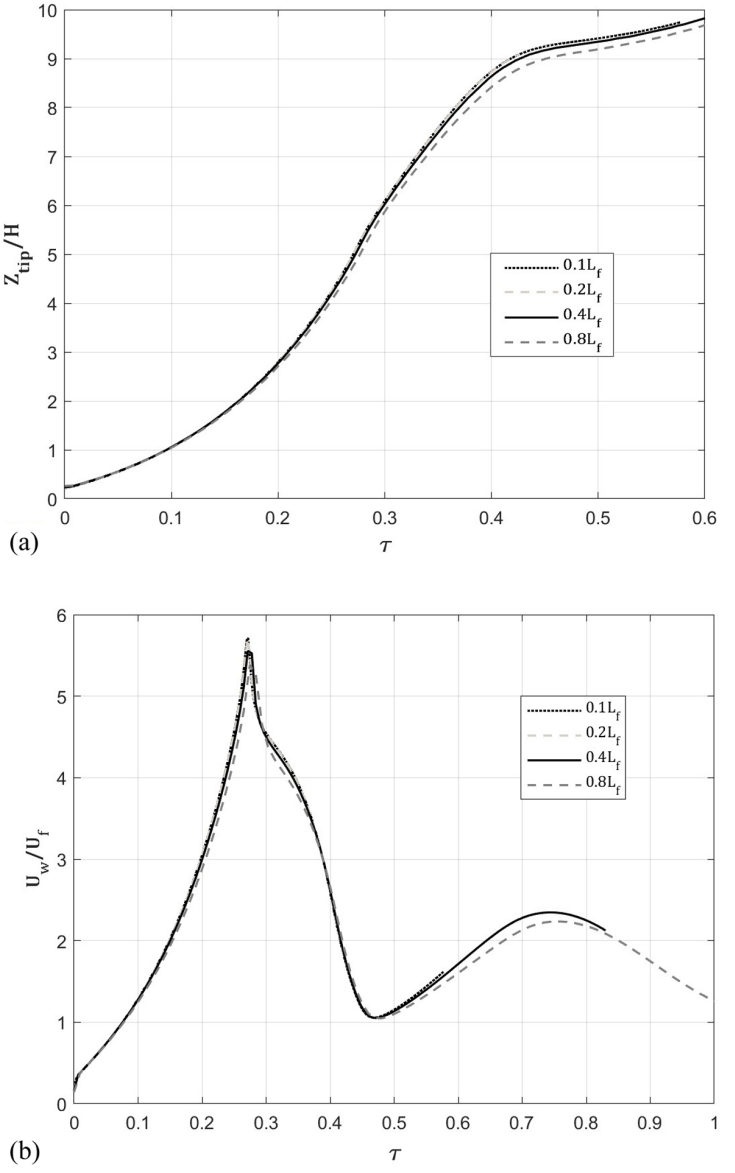

FIG. 2. The resolution test: The scaled flame-tip position Z_{tip}/H (a) and the scaled total burning rate U_w/U_f (b) vs the scaled time τ for different mesh sizes.

TABLE I. Resolution test.

$\Delta z_f/L_f$	$U_{w,\max}/U_f$	$\Delta U_{w,\max}/U_f$	$\tau_{U_w,\max}$	$\Delta\tau_{U_w,\max}$	(Z_{tip}/H)	$(\Delta Z_{\text{tip}}/H)$
0.8	5.384		0.2746		4.057	
0.4	5.556	0.172	0.2713	0.0033	4.185	0.128
0.2	5.706	0.150	0.2712	0.0001	4.233	0.048
0.1	5.714	0.008	0.2719	−0.0007	4.236	0.003

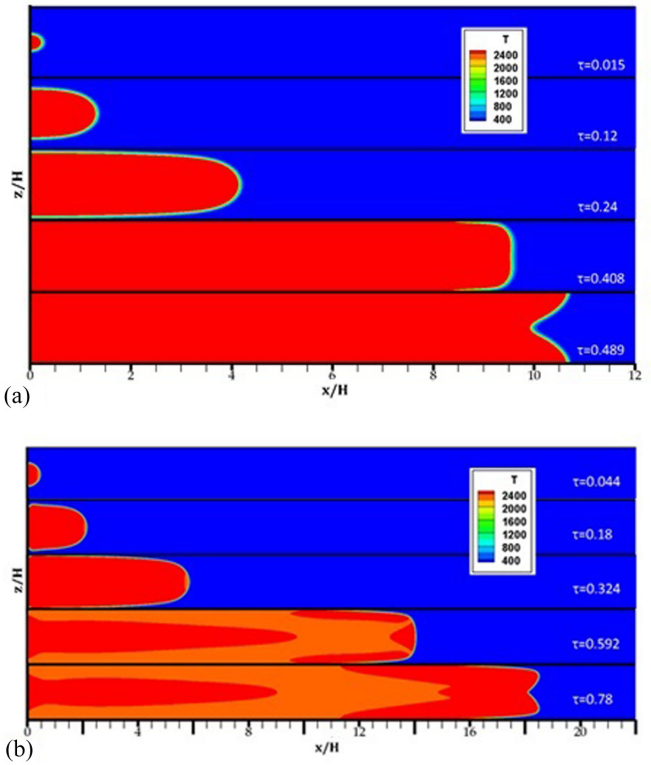

FIG. 3. Consecutive color temperature snapshots for the evolution of a $\Theta = 8$ flame in a channel of half-width $H = 30\ L_f$ with adiabatic, slip (a) and nonslip (b) walls.

thickness, which can be $4 \sim 5$ times larger [39,40]. Therefore, employing the grid of size $0.2\ L_f$, we actually have ∼20–25 cells inside the real flame thickness. It is also recalled that equidiffusive burning (the unity Lewis number, $\mathrm{Le} = 1$) is considered in this work such that isolines inside the flame are collinear, thereby diminishing the role of the internal flame structure. Otherwise, having $\mathrm{Le} < 1$ might promote the impact of the internal flame structure and might potentially require a refinement of the computational mesh.

III. RESULTS AND DISCUSSION

In the present section, we discuss the simulation results obtained for flame acceleration in channels with various walls boundary conditions and flow parameters. Specifically, in the first subsection, we employ both mechanistic, shear-stress (free-slip–nonslip) boundary conditions with adiabatic walls to examine the effect of wall friction on flame propagation for various channel half-widths, in the range $10 \leqslant H/L_f \leqslant 30$, and various thermal expansion ratios, in the range $5 \leqslant \Theta \leqslant 10$. Subsequently, in the second subsection, both thermal boundary conditions (adiabatic–isothermal) are employed and compared for various wall temperatures, in the range $298\ \mathrm{K} \leqslant T_w \leqslant 1000\ \mathrm{K}$, with free-slip walls and the same flow parameters as above—in order to distinguish the influence of heat losses on the flame dynamics and morphology.

A. Impacts of mechanistic boundary conditions

We start with Fig. 3 comparing the flame acceleration scenarios in channels of half-width $H = 30\ L_f$ with free-slip [Fig. 3(a)] and nonslip [Fig. 3(b)] walls. In both cases, the flame dynamics

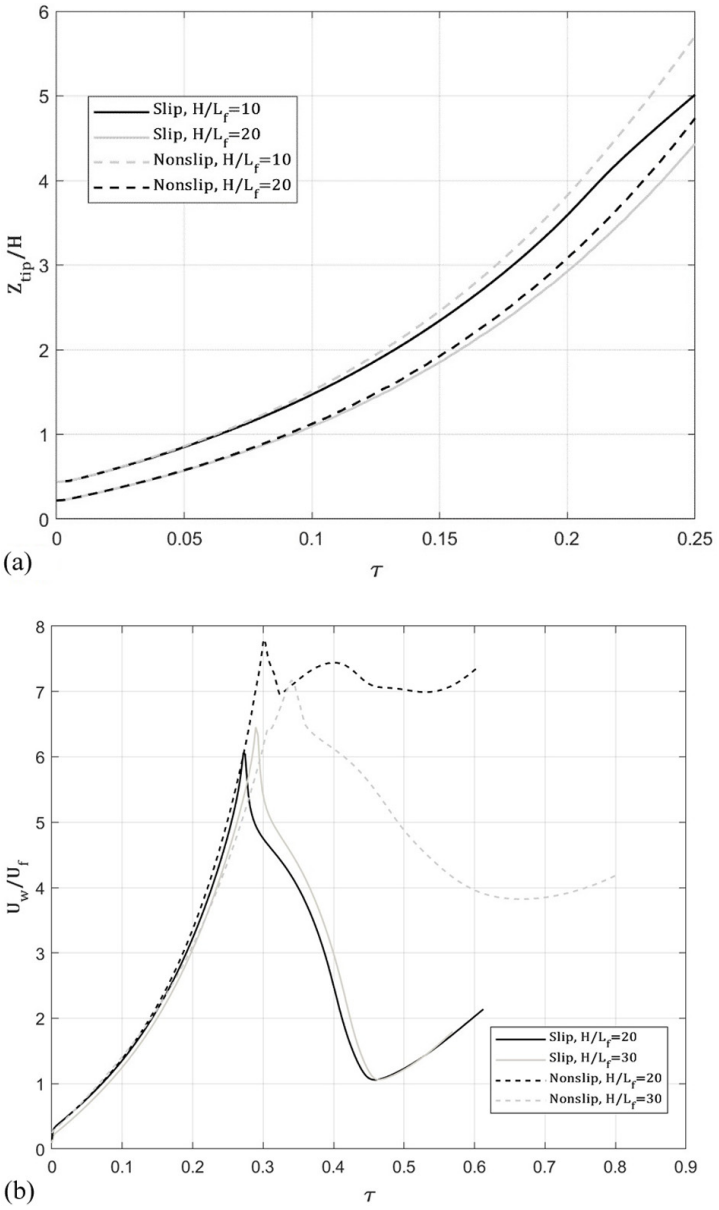

FIG. 4. The scaled flame-tip position Z_{tip}/H (a) and the scaled total burning rate U_w/U_f (b) vs the scaled time τ for the slip (solid) and nonslip (dashed) adiabatic walls for various channel half-widths.

exhibits a sequence of four stages, namely: (i) a hemispherical flame, (ii) a finger-shaped flame front, (iii) a quasiplanar flame and, eventually, (iv) an inverted concave tulip flame. The first stage occurs immediately after ignition when the flame embryo develops into a small hemispherical front that expands uniformly outwards. However, the flame front tends to spread in the x-direction, since expansion in the z-direction is limited by the sidewalls. As a result, the flame starts elongating. The second stage occurs as a result of such elongation, leading to an acquiring of a fingerlike flame shape, accompanied by the dramatic increase in the flame surface area (length in 2D) and the total burning rate. This finger flame acceleration stops when the flame skirt, which refers to the side

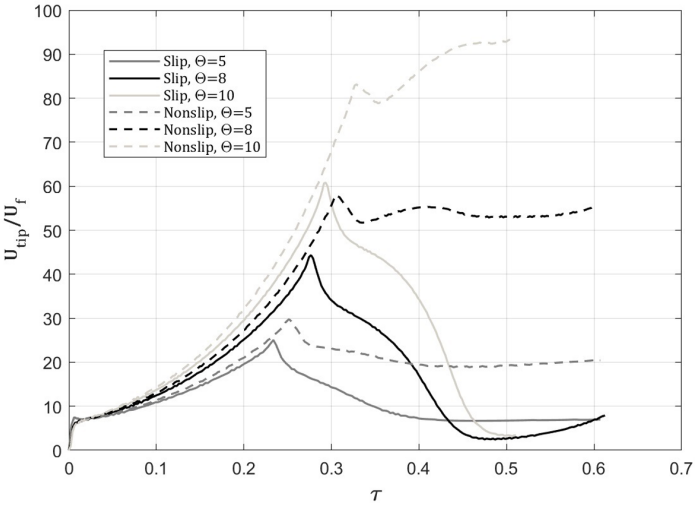

FIG. 5. The scaled flame-tip velocity U_{tip}/U_f vs the scaled time τ for the slip (solid) and nonslip (dashed) adiabatic walls with various thermal expansion ratios $\Theta = 5, 8, 10$.

segments of the flame front, contacts the sidewalls of the channel. At the next, third stage, the flame skirt forms small angles with the channel sidewalls; the flame velocity at these points then exceeds the laminar flame speed, which makes the flame skirt catching up the flame tip to form a quasiplanar flame. Finally, at the fourth stage, the flame front continues to decelerate, which is accompanied by a drastic decrease of the flame surface area. The flame front then inverts to form a cusp pointing backward or acquiring a tulip shape. This scenario agrees with the findings of Refs. [4,13,18].

As for the differences between the situations of slip and nonslip wall conditions, one of them is a corrugated flame shape at the closed end occurring due to wall friction at a nonslip wall. It is further noted that the temperature evolution is uniform during flame propagation for the slip walls, while some perturbations are seen for nonslip walls, when the flame front contacts a sidewall of the channel. Moreover, as the flame approaches the sidewalls, the effect of wall friction results in a corrugated tulip flame at the time instant $\tau = 0.78$; see the case of nonslip walls in Fig. 3(b). In summary, we would like to point out the nonmonotonic temperature field in the case of nonslip walls, Fig. 3(b). We devote this feature to viscous heating, thereby recognizing that a detailed study of viscous heating in this configuration may need to be undertaken elsewhere.

To quantify the qualitative, visual findings of Fig. 3, in Fig. 4, we present the time evolution of the scaled flame-tip position Z_{tip}/H (during the acceleration stage) [Fig. 4(a)] and of the scaled total burning rate U_w/U_f [Fig. 4(b)] for the channels of various half-widths in the cases of both slip and nonslip walls. Figure 4(a) shows that the impact of wall friction is minor during the acceleration stage, when a flame front acquires a finger shape. This minority can be explained by the fact that acceleration occurs at the centerline, i.e., away from the channel sidewalls. However, according to Fig. 4(b), as the flame skirt comes to a sidewall, in the case of nonslip walls, wall friction results in a noticeable increase in the total burning rate as compared to the event of free-slip walls, when the total burning rate decreases sharply.

We next analyzed the impact of such a key factor of premixture as thermal expansion in the burning process on finger flame acceleration. Specifically, we performed numerical simulations for different values of the thermal expansion ratio, namely, $\Theta = 5,\ 8,$ and 10, for the fixed channel half-width, $H = 20\, L_f$, with both slip and nonslip, adiabatic walls employed. The result is shown in Fig. 5, where the time evolutions of the scaled flame-tip velocity U_{tip}/U_f are compared for all these cases, with the solid and dashed lines devoted to the slip and nonslip walls, respectively. All the curves of Fig. 5 exhibit similar qualitative trends, with the initial expansion of a hemispherical

TABLE II. The maximal scaled flame-tip velocity and the maximal scaled total burning rate for different thermal expansion coefficients.

Mechanistic boundary condition	Θ	$U_{\mathrm{tip,max}}/U_f$	$\tau_{U_{\mathrm{tip}},\mathrm{max}}$	$U_{w,\mathrm{max}}/U_f$	$\tau_{U_w,\mathrm{max}}$
Slip	5	25.1	0.234	5.53	0.231
Nonslip	5	29.8	0.251	7.04	0.248
Slip	8	44.3	0.277	6.06	0.272
Nonslip	8	58.0	0.302	7.80	0.304
Slip	10	60.8	0.294	6.83	0.289
Nonslip	10	93.5	0.510	10.5	0.510

flame, followed by the elongation of a convex finger-shaped front, and ending with the formation of a concave, tulip flame. The flame-tip velocity increases with the thermal expansion ratio for both slip and nonslip walls. Furthermore, the flame shape is more corrugated in the presence of wall friction and, therefore, the maximal flame-tip velocity in the case of nonslip walls is higher than that in the event of slip walls. The maximal values for the scaled total burning rate and the scaled flame-tip velocity for slip and nonslip walls are also summarized in Table II.

B. Impacts of thermal boundary conditions

In order to examine the effect of thermal boundary conditions on the combustion process, the adiabatic walls, as well as the isothermal walls of various wall temperatures, are next employed and compared. We start with the color temperature snapshots of Fig. 6 representing the typical finger flame evolution scenarios in a channel of half-width $H = 20\ L_f$ with free-slip, isothermal walls. Specifically, Fig. 6(a) is devoted to the cold walls kept at the room temperature, $T_w = 298$ K, while the flame evolution in a channel with preheated walls, $T_w = 600$ K, is presented in Fig. 6(b). According to Fig. 6, a hemispherical flame expands, whereas its surface area and velocity increase dramatically until the flame skirt contacts the sidewalls and the heat losses cool down the flame such that the flame surface area and the total burning rate then decrease dramatically. A tulip flame is formed, followed by its evolution into a quasiplanar flame, which then collapses to acquire a curved convex shape of the front, presumably, because of the Darrieus-Landau instability [4,13].

The qualitative difference between the adiabatic and isothermal wall conditions can be seen when comparing Fig. 3(a), devoted to the slip adiabatic walls, to Figs. 6(a) and 6(b), representing the slip isothermal walls. Specifically, when the combustor walls are kept at a room temperature [Fig. 6(a)], the heat exchange occurs when the burnt matter expands, and heat is transferred from the combustor to the environment through the cold walls. The heat losses cause the flame skirt to cool down, where the region of the heat is then localized around the flame tip. The same effect is seen in Fig. 6(b), for the preheated walls, where the temperature of the burnt matter decreases. In contrast, we observed a uniform temperature evolution for flame propagation with adiabatic walls, because heat is conserved at the combustor walls in that case.

A quantitative difference between the flame propagation scenarios in adiabatic and isothermal channels is demonstrated in Fig. 7, where the scaled total burning rates U_w/U_f are compared for different thermal wall conditions. It is seen that thermal boundary conditions have a small impact on flame acceleration; the latter diminishes with the reduction of the wall temperature, but only slightly. This also can be explained by the fact that finger flame acceleration occurs away from the sidewalls, and the effect of heat losses emerges only when the flame skirt approaches the sidewalls.

An impact on the flame dynamics and morphology has been observed when the walls were further preheated. Specifically, Fig. 8 shows the temperature snapshots for the flame evolution in an isothermal channel with a high wall temperature, $T_w = 1000$ K. Here, as soon as a flame embryo is ignited at the centerline, at the closed end of the channel, and then expands toward the open end, additional flame segments are formed at the preheated walls. The fundamental cause of this feature

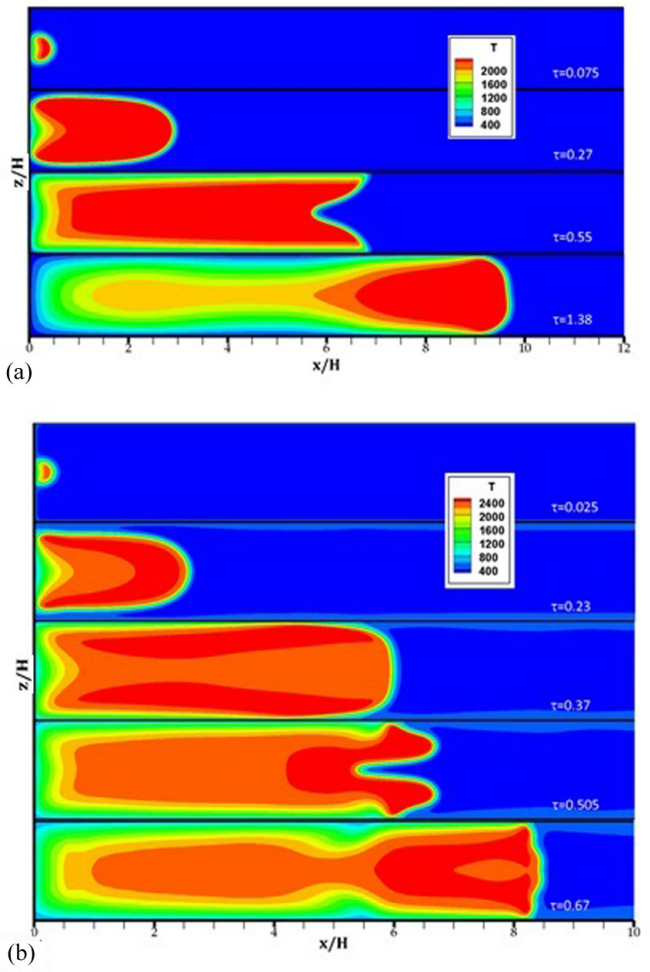

FIG. 6. Consecutive color temperature snapshots for the evolution of a $\Theta = 8$ flame in a channel of half-width $H = 20\, L_f$ with slip, isothermal walls: (a) cold, $T_w = 298$ K, and (b) preheated, $T_w = 600$ K.

is the hot regions near the sidewalls, which can initiate and facilitate the combustion process. The flame acquires a finger shape after the expansion of the hemispherical embryo, while the flame segments near the sidewalls also propagate toward the open end. This scenario eventually leads to an "octopus" shape of the flame front. Emergence and propagation of such an octopus are accompanied by an increase in the total burning rate and the flame surface area as compared to the previous cases, but this also occurs for a limited time. Indeed, the octopus then disappears when the secondary flame segments merge with the flame tip, which is followed by a decrease in the flame surface area. The flame subsequently acquires a quasiplanar shape of the front, and then a tulip flame is eventually formed as a result of the further reduction in the flame surface area. It is also seen that the tulip flame is more corrugated in this case than in Figs. 3 and 6, presumably, due to the higher temperature of the sidewalls as well as due to heat losses through the walls.

To quantify this effect, in Fig. 9 we compare the time evolutions of the scaled total burning rates in the cases of hot isothermal walls, $T_w = 800$ and 1000 K, as well as in the case of adiabatic walls. It is seen that the hot walls can facilitate the combustion process: a flame accelerates slightly faster when the wall temperature reaches, in particular, 1000 K as compared to the adiabatic case.

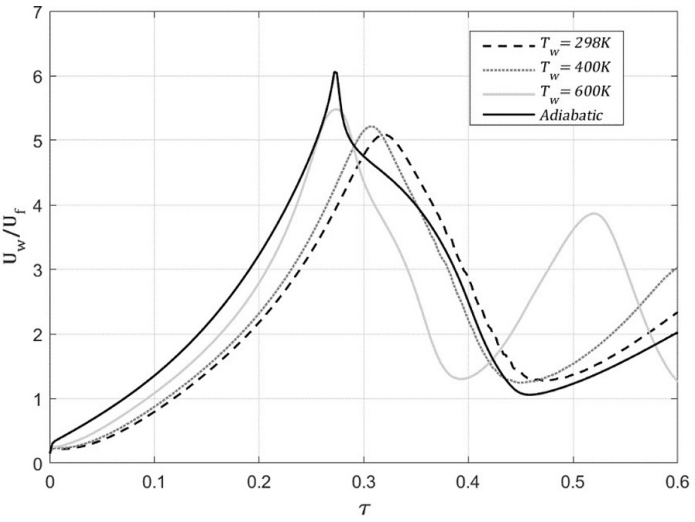

FIG. 7. The scaled total burning rate U_w/U_f vs the scaled time τ for a $\Theta = 8$ flame in a channel of half-width $H = 20\ L_f$ with adiabatic walls (solid) and isothermal walls (dashed) at various wall temperatures: $T_w = 298$, 400, and 600 K.

This can be explained by the fact that acceleration occurs away from the sidewalls, and the heat is transferred from the hot walls to the flame at this stage, before the flame front contacts the sidewall. In Table III, we summarize the maximal scaled burning rates and the maximal scaled flame-tip

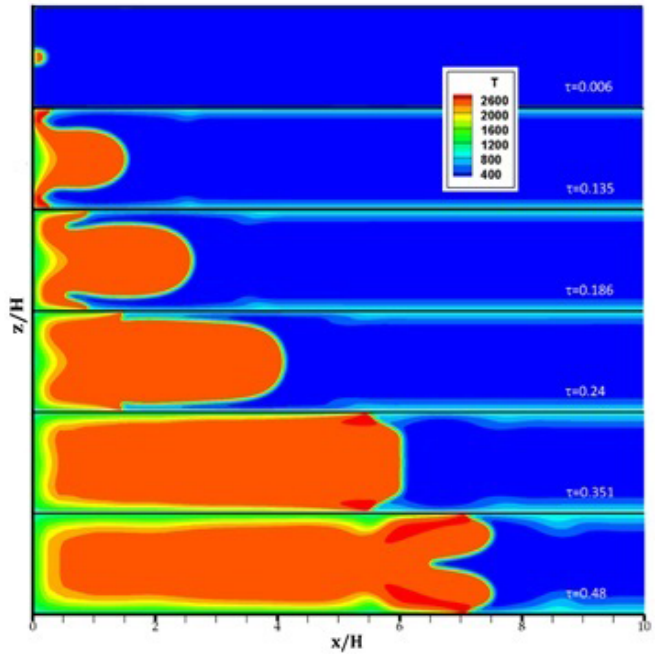

FIG. 8. Consecutive color temperature snapshots for the evolution of a $\Theta = 8$ flame in a channel of half-width $H = 30\ L_f$ with the slip, isothermal (preheated) walls at $T_w = 1000$ K: formation and disappearance of an octopus flame.

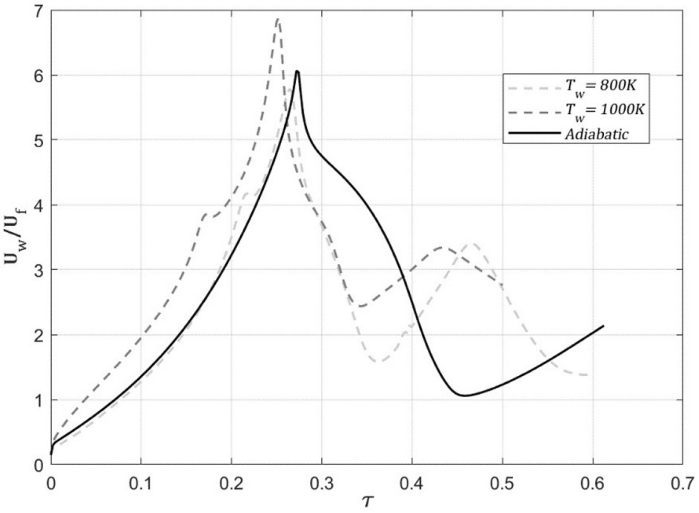

FIG. 9. The scaled total burning rate U_w/U_f vs the scaled time τ for a $\Theta = 8$ flame in a channel of half-width $H = 30\ L_f$ with the isothermal walls of wall temperatures $T_w = 800$ and 1000 K (dashed) as well as with the adiabatic walls (solid).

velocities for various wall conditions. It is seen that the flame-tip velocity and the total burning rate grow with the temperature of the walls, which also slightly promotes the acceleration rate.

We next investigate the impact of the channel size on the isothermal channels, where it is expected to play a greater role as compared to the adiabatic channels. For this purpose, Fig. 10 compares, quantitatively, U_w/U_f for different channel half-widths in the range $10 \leqslant H/L_f \leqslant 30$, in particular cases of a room, $T_w = 298$ K [Fig. 10(a)], and highly preheated, $T_w = 1000$ K [Fig. 10(b)], wall temperatures. It is seen that the role of the channel width is major for cold walls kept at an initial fuel temperature [Fig. 10(a)], especially as the channel half-width decreases to $H = 10\ L_f$, while the effect diminishes as H grows from $20\ L_f$ to $30\ L_f$. Moreover, the impact of the channel width on the acceleration rate is not significant in Fig. 10(a), since the flame approaches the sidewalls almost at the same scaled time instants, $\tau \approx 0.32$. On the other hand, the situation is a little different in Fig. 10(b) for the very hot isothermal walls, $T_w = 1000$ K. Here, the impact of the channel width on the total burning rate is notable, due to the fact that such hot walls facilitate the burning process by generating new flame segments, which is accompanied by the increase in the burning rate.

Let us next discuss the impact of thermal expansion on flame propagation at various thermal boundary conditions. Specifically, Fig. 11 shows the impact of a relatively high thermal expansion ratio, $\Theta = 10$, on the morphology and dynamics of a flame propagating in an isothermal

TABLE III. The maximal scaled flame-tip velocity and maximal scaled total burning rate for different thermal boundary conditions and wall temperatures.

Thermal boundary condition	T_w (K)	$U_{\text{tip,max}}/U_f$	$\tau_{U_{\text{tip}},\text{max}}$	$U_{w,\text{max}}/U_f$	$\tau_{U_w,\text{max}}$
Adiabatic		44.3	0.277	6.06	0.272
Isothermal	298	32.6	0.325	4.99	0.330
Isothermal	400	34.3	0.300	5.22	0.310
Isothermal	600	36.8	0.270	5.48	0.274
Isothermal	800	37.2	0.267	5.78	0.264
Isothermal	1000	40.7	0.254	6.88	0.252

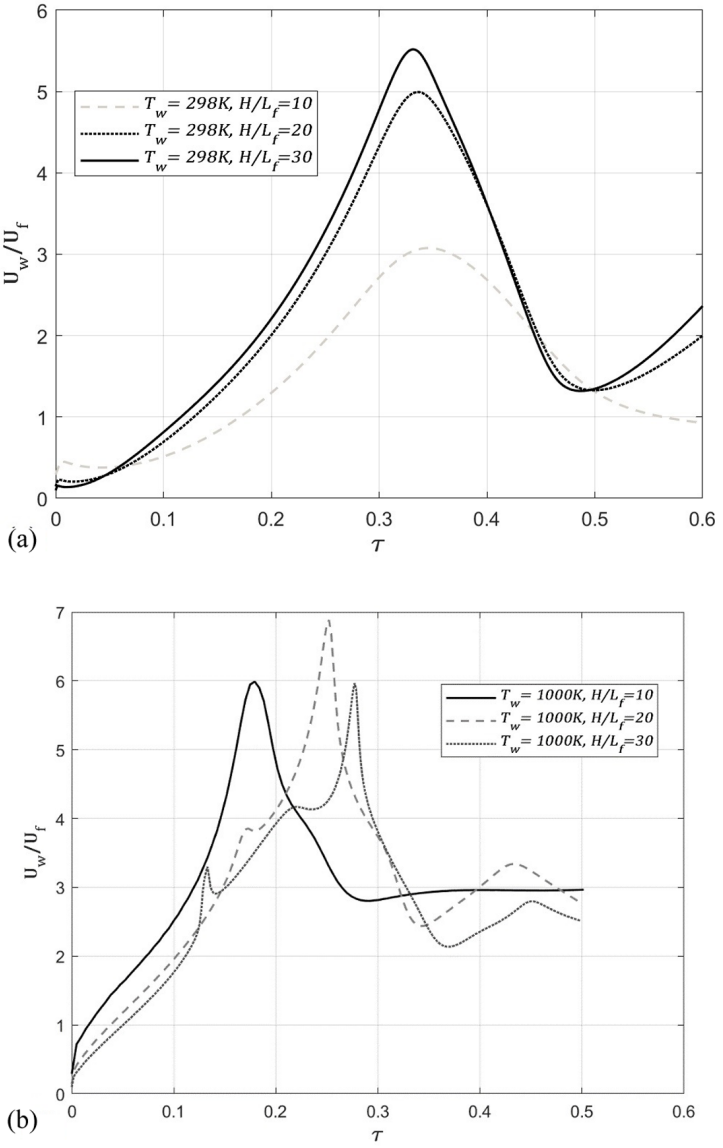

FIG. 10. The scaled total burning rate U_w/U_f vs the scaled time τ for a $\Theta = 8$ flame in the channels of half-widths $H/L_f = 10, 20, 30$ with the slip, isothermal walls: (a) cold, $T_w = 298$ K and (b) preheated, $T_w = 1000$ K.

($T_w = 600$ K) channel of half-width $H = 20\ L_f$. Overall, the flame dynamics is qualitatively the same as in the previous cases, i.e., the standard finger flame scenario is seen, with the initial expansion of a hemispherical flame front, followed by acceleration of a finger flame, and then deceleration and the formation of a tulip flame. The impact of a higher thermal expansion results in a more corrugated tulip flame, which experiences higher distortion of the front as the flame sweeps on the sidewalls.

Finally, Fig. 12 presents the scaled total burning rate U_w/U_f versus the scaled time τ, for the adiabatic walls [Fig. 12(a)] as well as the isothermal preheated walls at the wall temperatures of 400 K [Fig. 12(b)] and 600 K [Fig. 12(c)]. Here, we have the same channel half-width, $H = 20L_f$,

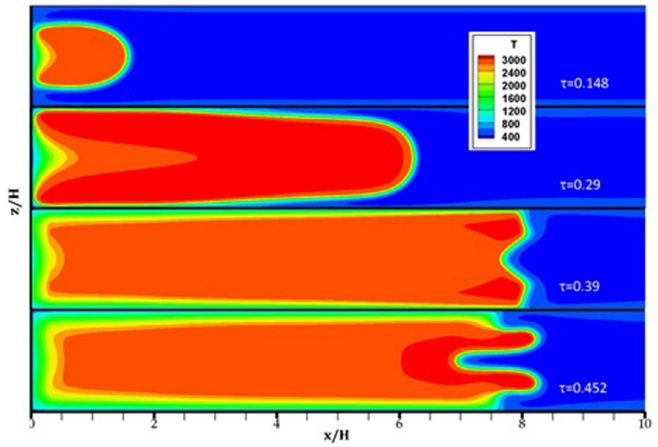

FIG. 11. Consecutive color temperature snapshots for the evolution of a $\Theta = 10$ flame in a channel of half-width $H = 20\,L_f$ with slip, isothermal (preheated) walls of wall temperature $T_w = 600$ K.

but various thermal expansion ratios in the range $5 \leqslant \Theta \leqslant 10$ in all cases. Overall, the adiabatic and isothermal cases look qualitatively very similar, though with some quantitative differences. To be more accurate, it is seen that the maximal burning rate slightly increases with Θ for adiabatic walls, while this effect is small in the case of isothermal walls. Furthermore, thermal expansion has an impact on flame acceleration as a flame approaches the sidewalls faster with lower Θ for both types of the thermal boundary conditions, especially for isothermal walls.

IV. SUMMARY

In this paper, we have studied premixed flame acceleration in 2D channels by means of numerical simulations of the reacting flow equations, with fully-compressible hydrodynamics, transport properties (heat conduction, diffusion, and viscosity), and a single-step Arrhenius chemical kinetics. To be specific, we have investigated the impacts of thermal (adiabatic–isothermal) and shear-stress (slip–nonslip) boundary conditions (as well as that of various flow parameters such as the thermal expansion ratio, the wall temperature, and the channel width) on finger flame acceleration—an acceleration mechanism devoted to a situation when a premixed flame front acquires a finger shape, after an expansion of an embryonic hemispherical flame [4,13,18].

It is shown that the surface boundary conditions provide only small corrections during the early stages of burning, before a flame skirt contacts the wall. Indeed, the same qualitative flame dynamics was observed for slip and nonslip walls during the acceleration regime. This can be devoted to the fact that a flame is ignited and accelerates at the centerline of the channel, i.e., away from the sidewalls. However, the effect of wall friction can be observed as the flame approaches the sidewalls, where a distortion of the tulip flame occurs due to wall friction in the case of nonslip walls. After this stage, a flame front can propagate in the same manner as described by the classical Shelkin mechanism associated with wall friction at the nonslip walls [21]. Namely, the flame may keep accelerating until a detonation triggering. Furthermore, we have identified the effect of the thermal expansion ratio Θ, which facilitates the acceleration process. At the same time, the channel width has a small effect on flame propagation in both cases of slip or nonslip wall conditions.

The impacts of the thermal wall boundary conditions have been also scrutinized. It is observed that the finger flame dynamics in adiabatic channels is similar to that in isothermal channels. This is also because of heat losses occurring during the deceleration regime, when a more distorted tulip flame is formed due to the lost thermal energy. It is also shown that the wall temperature T_w has an impact on flame acceleration such that a flame tends to accelerate faster when T_w grows. Moreover,

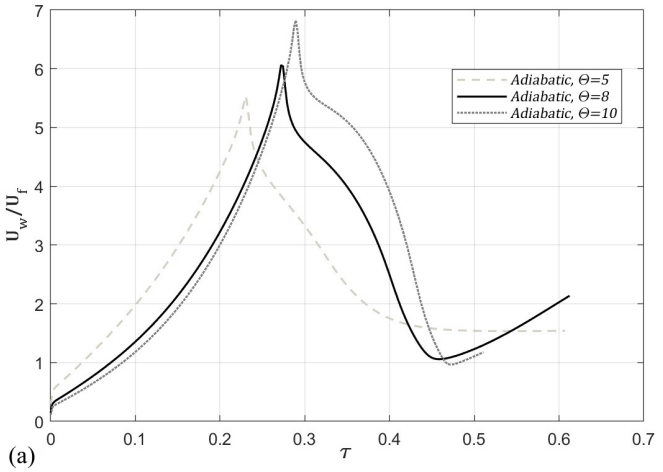

(a)

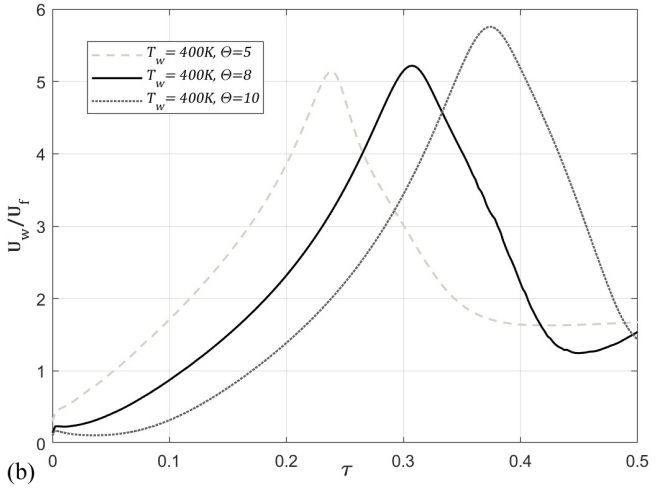

(b)

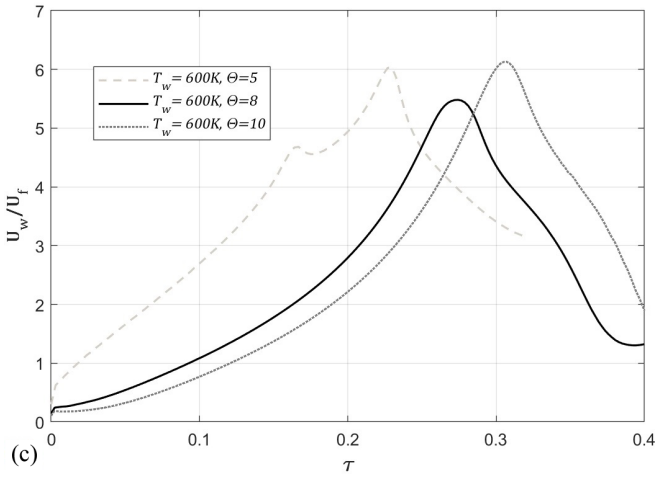

(c)

FIG. 12. The scaled total burning rate U_w/U_f vs the scaled time τ for the flames of various thermal expansion ratios $\Theta = 5, 8, 10$ propagating in a channel of half-width $H = 20\ L_f$ with adiabatic walls (a) and with isothermal (preheated) walls of wall temperatures $T_w = 400$ K (b) and 600 K (c).

for the isothermal walls preheated to a high temperature, $T_w = 1000$ K, we observed an interesting stage of an octopuslike flame propagation; see Fig. 8. This phenomenon occurs due to the formation of secondary flame segments, near the sidewalls, due to the high wall temperature. Subsequently, the octopus disappears, and a tulip flame is formed, when these flame segments merge with the flame tip. Furthermore, the channel size has a small impact on the adiabatic walls, but it provides a significant influence on the growth trend of the total burning rate and the flame-tip velocity for the flames propagating in the channels with isothermal cold walls. This can be explained by the fact that the produced energy diminishes with the reduction of the channel width. On the other hand, this effect is small for hot walls, as heat is gained from the hot combustor walls at the early stages of the burning process. Finally, we have scrutinized the effect of thermal expansion on both types of the thermal boundary conditions. The impact of Θ on acceleration is slightly higher in the case of isothermal walls, and the flames approach the sidewalls faster with lower Θ. The latter can presumably be devoted to the fact that more thermal energy is lost for higher thermal expansion ratios, which promotes slower flame acceleration.

ACKNOWLEDGMENTS

This study at West Virginia University was sponsored by the U.S. National Science Foundation (NSF) through the CAREER Award No. 1554254 (V.A.) as well as by the West Virginia Higher Education Policy Commission through Grant No. HEPC.dsr.18.7 (V.A.). D.V. was supported by the National Science Foundation of China (NSFC) through Grant No. 52176118.

[1] G. D. Roy, S. M. Frolov, A. A. Borisov, and D. W. Netzer, Pulse detonation propulsion: Challenges, current status and future perspective, Prog. Energy Combust. Sci. **30**, 545 (2004).

[2] D. P. Nolan, *Handbook of Fire and Explosion Protection Engineering Principles* (William Andrew/ Elsevier, Kidlington, UK, 2004).

[3] G. Ciccarelli and S. Dorofeev, Flame acceleration and transition to detonation in ducts, Prog. Energy Combust. Sci. **34**, 499 (2008).

[4] C. Clanet and G. Searby, On the "tulip flame" phenomenon, Combust. Flame **105**, 225 (1996).

[5] K. I. Schelkin, The impact of the tube wall roughness on the emergence and propagation of a detonation in gases, Zh. Eksp. Teor. Fiz. **10**, 823 (1940).

[6] O. Ugarte, V. Bychkov, J. Sadek, D. Valiev, and V. Akkerman, Critical role of blockage ratio for flame acceleration in channels with tightly spaced obstacles, Phys. Fluids **28**, 093602 (2016).

[7] O. Ellis, Flame movement in gaseous explosive mixtures, Fuel Sci. Pract. **VII**, 502 (1928).

[8] G. Salamandra, T. Bazhenova, and I. Naboko, Formation of detonation wave during combustion of gas in combustion tube, Proc. Combust. Inst. **7**, 851 (1959).

[9] D. Rotman and A. Oppenheim, Aerothermodynamic properties of stretched flames in enclosures, Proc. Combust. Inst. **21**, 1303 (1988).

[10] M. Gonzalez, Acoustic instability of a premixed flame propagating in a tube, Combust. Flame **107**, 245 (1996).

[11] F. Marra and G. Continillo, Numerical study of premixed laminar flame propagation in a closed tube with a full Navier-Stokes approach, Proc. Combust. Inst. **26**, 907 (1996).

[12] D. Dunn-Rankin and R. Sawyer, Tulip flames: Changes in shape of premixed flames propagating in closed tubes, Exp. Fluids **24**, 130 (1998).

[13] V. Bychkov, V. Akkerman, G. Fru, A. Petchenko, and L.-E. Eriksson, Flame acceleration in the early stages of burning in tubes, Combust. Flame **150**, 263 (2007).

[14] H. Xiao, Q. Wang, X. He, J. Sun, and X. Shen, Experimental study on the behaviors and shape changes of premixed hydrogen-air flames propagating in horizontal duct, Int. J. Hydrogen Energy **36**, 6325 (2011).

[15] H. Xiao, Q. Wang, X. Shen, W. An, Q. Duan, and J. Sun, An experimental study of premixed hydrogen-air flame propagation in a partially open duct, Int. J. Hydrogen Energy **39**, 6233 (2014).
[16] H. Xiao, R. Houim, and E. Oran, Formation and evolution of distorted tulip flames, Combust. Flame **162**, 4084 (2015).
[17] M. Kuznetsov, V. Alekseev, I. Matsukov, and S. Dorofeev, DDT in a smooth tube filled with a hydrogen-oxygen mixture, Shock Waves **14**, 205 (2005).
[18] D. Valiev, V. Akkerman, M. Kuznetsov, L.-E. Eriksson, C. K. Law, and V. Bychkov, Influence of gas compression on flame acceleration in the early stage of burning in tubes, Combust. Flame **160**, 97 (2013).
[19] S. Demir, V. Bychkov, S. H. R. Chalagalla, and V. Akkerman, Towards a predictive scenario of a burning accident in a mining passage, Combust. Theor. Model. **21**, 997 (2017).
[20] S. Demir, A. R. Calavay, and V. Akkerman, Influence of gas compression on a burning accident in a mining passage, Combust. Theor. Model. **22**, 338 (2018).
[21] V. Bychkov, A. Petchenko, V. Akkerman, and L.-E. Eriksson, Theory and modeling of accelerating flames in tubes, Phys. Rev. E **72**, 046307 (2005).
[22] W. Han, Y. Gao, and C. K. Law, Flame acceleration and deflagration-to-detonation transition in micro- and macro-channels: An integrated mechanistic study, Combust. Flame **176**, 285 (2017).
[23] M. Ivanov, A. Kiverin, and M. Liberman, Flame acceleration and DDT of hydrogen-oxygen gaseous mixtures in channels with no-slip walls, Int. J. Hydrogen Energy **36**, 7714 (2011).
[24] E. Dzieminska and A. K. Hayashi, Auto-ignition and DDT driven by shock wave–boundary layer interaction in oxyhydrogen mixture, Int. J. Hydrogen Energy **38**, 4185 (2013).
[25] T. Machida, M. Asahara, A. K. Hayashi, and N. Tsuboi, Three-dimensional simulation of deflagration-to-detonation transition with a detailed chemical reaction model, Combust. Sci. Technol. **186**, 1758 (2014).
[26] M. Ivanov, A. Kiverin, I. Yakovenko, and M. Liberman, Hydrogen-oxygen flame acceleration and deflagration-to-detonation transition in three-dimensional rectangular channels with no-slip walls, Int. J. Hydrogen Energy **38**, 16427 (2013).
[27] L. Kagan, D. Valiev, M. Liberman, and G. Sivashinsky, Effect of hydraulic resistance and heat losses on the deflagration-to-detonation transition, in *Pulse Detonation Engine* (Torus Press Ltd., Moscow, 2006), pp. 51–62.
[28] V. Gamezo and E. Oran, *Flame Acceleration in Narrow Tubes: Effect of Wall Temperature on Propulsion Characteristics*. The 44th AIAA Aerospace Sciences Meeting and Exhibit, Reno, NV, Jan. 9–12 (2006).
[29] J. D. Ott, E. S. Oran, and J. D. Anderson, A mechanism for flame acceleration in narrow tubes, AIAA J. **41**, 1391 (2003).
[30] C. L. Hackert, J. L. Ellzey, and O. A. Ezekoye, Effects of thermal boundary conditions on flame shape and quenching in ducts, Combust. Flame **112**, 73 (1998).
[31] I. Brailovsky and G. Sivashinsky, Hydraulic resistance as a mechanism for deflagration-to-detonation transition, Combust. Flame **122**, 492 (2000).
[32] D. Norton and D. Vlachos, *Combustion* characteristics and flame stability at the microscale: A CFD study of premixed methane/air mixtures, Chem. Eng. Sci. **58**, 4871 (2003).
[33] J. Daou and M. Matalon, Influence of conductive heat-losses on the propagation of premixed flames in channels, Combust. Flame **128**, 321 (2002).
[34] G. P. Gauthier and J. M. Bergthorson, Effect of external heat loss on the propagation and quenching of flames in small heat-recirculating tubes, Combust. Flame **173**, 27 (2016).
[35] O. Ugarte and V. Akkerman, Computational study of premixed flame propagation in micro-channels with nonslip walls: Effect of wall temperature, Fluids **6**, 36 (2021).
[36] C. Dion, D. Valiev, V. Akkerman, B. Demirgok, O. Ugarte, L.-E. Eriksson, and V. Bychkov, Dynamics of flame extinction in narrow channels with cold walls: Heat loss versus acceleration, Phys. Fluids **33**, 033610 (2021).
[37] C. Wang, Y. Zhao, and W. Han, Effect of heat-loss boundary on flame acceleration and deflagration-to-detonation transition in narrow channels, Combust. Sci. Technol. **189**, 1605 (2017).

[38] W. Han, J. Huang, G. Gu, C. Wang, and C. K. Law, Surface heat loss and chemical kinetic response in deflagration-to-detonation transition in microchannels, Phys. Rev. Fluids **5**, 053201 (2020).

[39] R. J. Blint, The relationship of the laminar flame width to flame speed, Combust. Sci. Technol. **49**, 79 (1986).

[40] V. Akkerman, V. Bychkov, A. Petchenko, and L.-E. Eriksson, Flame oscillations in tubes with non-slip at the walls, Combust. Flame **145**, 675 (2006).

[41] H. K. Versteeg and W. Malalasekera, *An Introduction to Computational Fluid Dynamics. The Finite Volume Method*, 2nd ed. (Pearson/Prentice Hall, Harlow, 2007), p. 295.